EXAFS evidence for a primary Zn_{Li} dopant in $LiNbO_3$

F. Bridges,[1,2] J. Castillo-Torres,[3] B. Car,[1] S. Medling,[1] and M. Kozina[1]

[1]*Physics Department, University of California, Santa Cruz, California 95064, USA*

[2]*Department of Microtechnology and Nanoscience, Chalmers University of Technology, SE-41296 Gothenburg, Sweden*

[3]*Instituto de Física y Matemáticas, Universidad Tecnológia de la Mixteca, Carretera a Acatlima Km 2.5, CP 69000,*
Huajuapan de León Oaxaca, Mexico

We present extended x-ray-absorption fine structure (EXAFS) data as a function of temperature (10–300 K) at the Zn and Nb K edges for Zn-doped $LiNbO_3$. The focus is on higher Zn concentrations (7–11 mol %) for which there is disagreement in the literature as to the substitution site for Zn. Our data show that Zn substitutes only on the Li site; we find no evidence for Zn on the Nb site. However, uncertainties result in an upper bound of at most 5% of the Zn dopants being Zn_{Nb}. In addition, the Zn_{Li} defect produces a significant distortion in the lattice out to at least 4 Å; the O atoms are attracted toward Zn while the Nb neighbors are repulsed. The Nb EXAFS agree well with the structure from diffraction for the main Nb-X peaks out to about 3.7 Å. However, there appears to be a weak third Nb-O peak in the first O shell, which has a low amplitude and a longer bond length. For Nb, the shortest Nb-O bond is extremely stiff (correlated Debye temperature, $\theta_{cD} \sim 1100$ K), while the longer Nb-O bond is a little weaker ($\theta_{cD} \sim 725$ K) and of comparable strength to the shortest Zn-O bond ($\theta_{cD} \sim 600$ K); consequently, substituting Zn at the Li site will stiffen the structure as the Li-O bonds are weak. We discuss implications of a dominant Zn_{Li} defect.

PACS number(s): 61.05.cj, 61.72.J−

I. INTRODUCTION

Lithium niobate, $LiNbO_3$ (LNO), is one of the most technologically relevant materials for acoustic and optical applications. It is a dielectric ceramic and is very versatile because of its large piezoelectric, acousto-optic, pyroelectric, electro-optic, photoconductive, ferroelectric, photorefractive, and nonlinear optical parameters.[1] LNO has been called the "optical silicon" since it has been used in a wide range of applications, including photorefractive devices, solid-state lasers, waveguides, optical storage, modulators, switches, and filters.[2] Many of these properties can be modified or controlled by specific dopants. For example, when dopants such as Mg, Zn, In, or Hf are incorporated in LNO, the material becomes more resistive to optical-damage,[3,4] i.e., a decrease in its photorefractive response appears, and then one can take advantage of its other properties such as optical frequency conversion (second harmonic generation).[5] However, to fully understand the microscopic mechanisms for the suppression of the photorefractive effect and to determine the precise nature of donors and acceptors, the dopant site location (on Li^+ or Nb^{+5}) and the local environment about the active transition-metal impurities has to be elucidated. Congruent LNO is not stoichiometric with an excess of Nb, and it is likely that the presence of nonstoichiometric defects is one of the reasons why LNO tolerates a strong incorporation of dopants that are nonisovalent to either Li^+ and Nb^{+5}.

There have been many efforts—both theoretical[5–14] and experimental[3,15–32]—to investigate intrinsic and extrinsic defects. For undoped, congruent LNO each antisite $Nb_{Li}^{\bullet\bullet\bullet\bullet}$ is compensated by 4 Li vacancies V_{Li}' in Kröger-Vink notation, i.e., $[Li_{1-5x}Nb_x V_{4x}][Nb]O_3$.[6] Adding divalent and/or trivalent metal dopants produces extrinsic defects that modify important optical properties and also change the lattice constants,[17,30] particularly near and above the so-called threshold concentration of ~ 7 mol %. For Zn dopants, nearly all studies suggest that at Zn concentrations below ~ 5–6 mol %, Zn substitutes on the Li site, mainly for Nb_{Li} and V_{Li} defects in congruent LNO.[17–22,30]

Above 6–7 mol % Zn, however, a number of investigations, particularly diffraction studies, have proposed that Zn goes onto both Li and Nb sites[17,19,21,30,33] to explain structural and density changes as well as the optical changes. In many studies, a self-compensation mechanism is proposed; that is, a simultaneous incorporation of Zn onto both Li and Nb sites achieves charge compensation without any change in oxygen. Chernaya *et al.*[19] suggests that at 7.6 mol % Zn, Zn_{Nb} defects already exist with Zn_{Nb}''' compensated by 3 $Zn_{Li}^{\bullet}$, i.e., $[Li_{1-3y}Zn_{3y}][Nb_{1-y}Zn_y]O_3$. Abdi *et al.*[17] propose that at 8.2 mol % Zn, even more Zn_{Nb} defects exist, with only 60% of the Zn dopants occupying Li sites, and the rest incorporated on Nb sites. However, some coercive field measurements[22] are not quantitatively in agreement with the above self-compensation model. In addition, pseudo-Schottky defect formation, i.e., Li^+ and O^{-2} vacancies, may not be completely ruled out.[30]

Unfortunately, such measurements are quite indirect and very few direct local structure measurements have been made. Room-temperature (RT) measurements for very dilute (<1 mol %) Ti^{+4} and Ni^{+2} suggest substitution mainly at the Li site[15] while similar RT measurements on Hf- and Hf/Mg-doped samples indicate that 1 mol % Hf substitutes at the Li when no Mg is present but at large Mg dopings (6 mol % Mg) the Hf substitutes on Nb sites.[16] One Zn EXAFS (extended x-ray absorption fine structure) experiment[23] did show Zn K-edge data at room temperature that indicated little change in the EXAFS with increasing Zn composition; they reported substitution on the Li site but no analysis was given. Instead they focused more on the Nb K-edge EXAFS data, and proposed a Nb vacancy model with five Zn_{Li} surrounding the vacancy ($5Zn_{Li}^{\bullet} + V_{Nb}''''')$.

Relatively few theoretical calculations have been carried out for dopants in congruent materials. Recently Xu *et al.*[14] have calculated the defect energies for several 2+ and 3+ metal atoms for various defect models in both congruent and stoichiometric materials, but did not consider Zn dopants explicitly. For 2+ dopants the model $Zn_{Li} + V_{Li}$ generally has the lowest formation energy in congruent materials while the self-compensated defect, $3Zn_{Li} + Zn_{Nb}$, has the lowest energy for stoichiometric materials. The latter is consistent with the earlier extensive study of many different dopants in stoichiometric materials in the dilute limit.[8]

In this work, a detailed analysis of Zn K-edge EXAFS spectra from 10 to 300 K has been carried out for Zn-doped LNO in order to clarify the lattice site location and to measure distances to the first few neighbors surrounding Zn. The focus for this study is on higher Zn concentrations (7–11 mol %) where discrepancies exist in the literature. Using the temperature dependence we can determine the relative strength of the bonds and the extent of any static disorder. Surprisingly for all samples, Zn substitutes only on the Li site—EXAFS is remarkably sensitive to the site location as discussed in the next section. Further, the environment about Zn is relatively distorted out to at least the third to fourth neighbors—the Nb neighbors about the Zn defect are pushed away.

We also report Nb K-edge data for the Zn-doped LNO, and also some other samples with low dopings of Mg and In, to ascertain how well the local structure about Nb agrees with the average structure from diffraction. Overall, the agreement is very good but there appears to be a small difference for the first Nb-O shell.

II. SIMPLE SUBSTITUTION SITES FOR ZN

As discussed above, several different models have been proposed for possible Zn centers in $LiNbO_3$; however, most involve Zn substitution on either the Li site (Zn_{Li}), the Nb site (Zn_{Nb}), both sites, clusters, or possibly the interstitial site (Zn_i) located along the c axis between Nb and Li. We first discuss simple substitutions before considering possible clusters. In Figs. 1 and 2 we show the first few shells of neighbors about the Li and Nb sites, respectively. Note that for Zn_{Li}, there are four Nb neighbors at a distance of ~3.06 Å, and additional Nb neighbors at 3.36 and 3.88 Å. The closest Li neighbors to Zn_{Li} are quite far away at 3.77 Å. In contrast, for Zn_{Nb}, the four closest metal neighbors are Li atoms at ~3.06 Å and the closest Nb neighbors are far away at 3.77 Å. For each site the first O shell has two Zn-O bond lengths, 0.2–0.27 Å apart. More details are provided in Table I.

If clusters form, with Zn on several nearby Li sites, then one must include a small number of Zn_{Li} as nearby neighbors to the central Zn atom. Also, if there is substitution on both sites and the Zn_{Li} and Zn_{Nb} sites are close together, then the local structure becomes more complex. This will be addressed in more detail when the data are fit to a model. We also briefly considered the interstitial site Zn_i, located roughly halfway between the Li and Nb atoms that are 3.88 Å apart along the c axis (vertical axis) in Figs. 1 and 2. Simulations for this site did not look at all similar to the experimental data and the Zn_i site was not considered further.
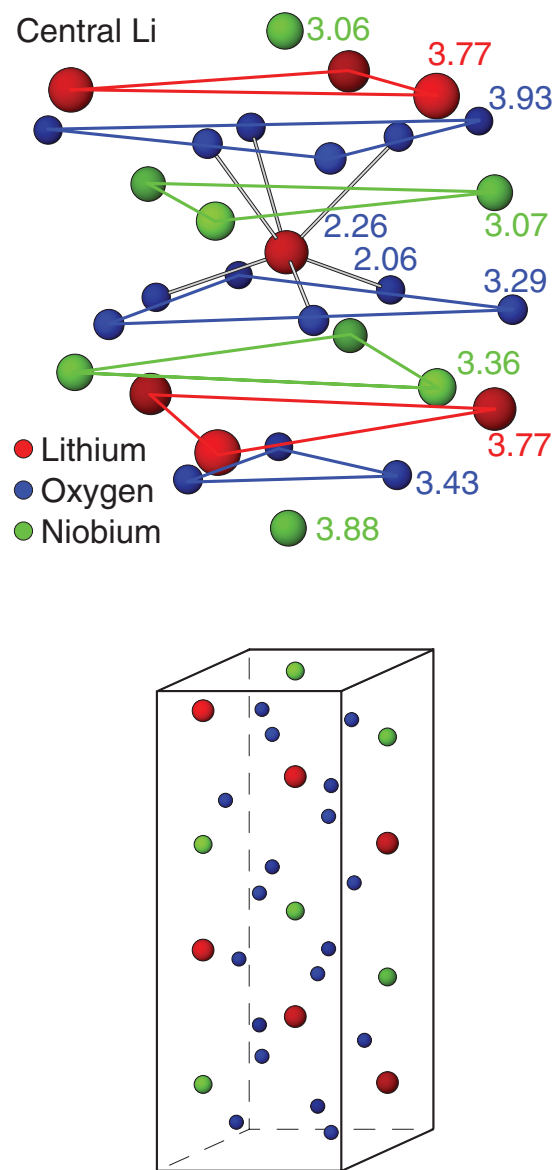

FIG. 1. (Color online) Top: The environment about the central Li site (large, red) in $LiNbO_3$. Bonds are shown for the nearest O atoms; other O shells are shown as small (blue) atoms. The four medium (green) atoms (three in a plane) above the central atom are Nb at ~3.07 Å; a second plane of Nb atoms is below the center at 3.36 Å, while the bottom Nb atom is 3.88 Å below center. There are six Li (red) neighbors (three above and three below center) at 3.77 Å. Bottom: the hexagonal unit cell for $LiNbO_3$. The cluster above covers the top half of this cell but is expanded in the horizontal directions.

In EXAFS, the incident x-rays eject photoelectrons from the element of interest, when the appropriate x-ray energy is used. For Zn, this occurs above the K edge at 9660 eV. These photoelectrons are then backscattered from various shells of neighboring atoms, to produce oscillations in the absorption coefficient above the K edge. For $LiNbO_3$, the large difference in atomic number between Li ($Z = 3$) and Nb ($Z = 41$) plays a very important role, as the backscattering amplitude of this photoelectron from neighboring atoms depends strongly on the number of electrons present.
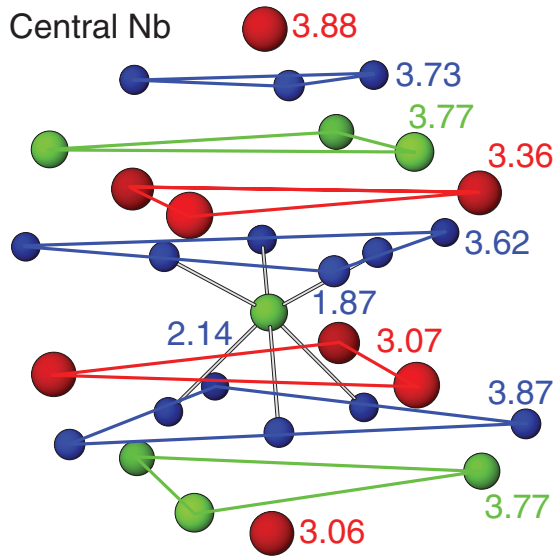
FIG. 2. (Color online) The environment about the central Nb site (green) in LiNbO$_3$. Bonds are shown for the nearest O atoms; again other O shells are shown as small (blue) atoms. The four red atoms (three in a plane) below the central atom are Li at ~3.07 Å; a second plane of Li atoms is above the center at 3.36 Å. There are six Nb (green) neighbors, three above and three below center, at 3.77 Å. The central Nb atom is at the center of the unit cell shown in Fig. 1.

Consequently, EXAFS is unusually sensitive to the Zn site location. Theoretical EXAFS functions, calculated for one neighbor at a distance 3.06 Å, are plotted for Zn-Li, Zn-Zn, and Zn-Nb pairs in Fig. 3. The Zn-Li peak is very small, only 8% of that for the Zn-Nb peak. As a result, Nb will dominate the EXAFS spectra beyond the first Zn-O shell—i.e., the largest peak(s) will correspond to Nb neighbors. The Zn-Zn peak amplitude is also more than ten times larger than for Zn-Li. Thus if significant clustering occurs such that Zn has two Zn neighbors, that will also be visible.

Using the known structure for LiNbO$_3$, one can easily simulate the EXAFS data for simple site substitution using the program FEFF8.[34] The FEFF8 program calculates the EXAFS k-space function for all paths. To be realistic we must also include a small global broadening for all peaks; here we used $\sigma = 0.06$ Å. The k-space functions were then Fast Fourier Transformed to r space. The r-space simulations for substitution on the Li and Nb sites are plotted in Figs. 4 and 5. Note that the largest peak (marked by the solid vertical lines) will occur near 2.8 Å if Zn is on the Li site, but near 3.5 Å if Zn is on the Nb site. This provides a rough fingerprint for

TABLE I. Pair distances for Zn substituted on either the Li or the Nb sites in LiNbO$_3$, assuming no distortion of the LNO lattice.

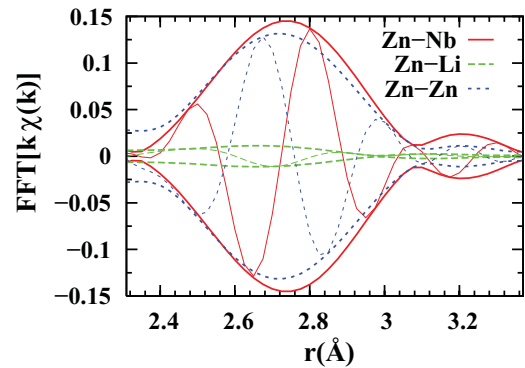| Li site		Nb site	
Atom pair	r(s) (Å)	Atom pair	r(s) (Å)
Zn-O	2.06,2.26	Zn-O	1.87,2.14
Zn-O	3.29,3.43,3.93	Zn-O	3.62,3.73,3.87
Zn-Nb	3.06,3.07	Zn-Li	3.06,3.07
Zn-Nb	3.36,3.88	Zn-Li	3.36,3.88
Zn-Li	3.77	Zn-Nb	3.77

FIG. 3. (Color online) Theoretical EXAFS functions calculated using FEFF8 for one neighbor of Li, Zn, or Nb, at a distance 3.07 Å from a central Zn atom. The Zn-Li peak is only 8% of the Zn-Nb peak; the Zn-Zn peak is also large, about 90% of the Zn-Nb peak. Note that the Zn-Li peak has a larger shift to lower r than the higher atomic number neighbors.

determining the Zn substitution site. Also the first two Zn-O peaks are shorter for the Nb site compared to the Li site.

III. EXPERIMENTAL DETAILS AND EXAFS TECHNIQUE

EXAFS data were collected for Zn-doped LiNbO$_3$ at the Zn K edge in fluorescence and transmission mode and at the host Nb K edge in transmission mode on beam line 10-2 at the Stanford Synchrotron Radiation Lightsource (SSRL). Data were collected over a range of temperatures from 10 to 300 K in an Oxford He cryostat. Three traces were collected for each sample and each temperature for both edges. For the Zn K edge, we used a double Si(111) monochromator, with a slit size of 0.5 mm by 10 mm, giving an energy resolution (δE) of 1.9 eV. To reduce the harmonic content in the x-ray beam, we detuned the monochromator crystals 50% at 9800 eV. For the high-energy Nb K edge we used a Si(220) double monochromator, detuned to 70% of maximum at 19 200 eV;
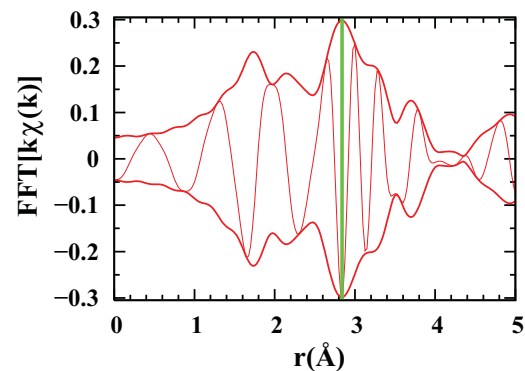

FIG. 4. (Color online) A simulation of the EXAFS r-space data [Fast Fourier Transform (FFT)[$k\chi(k)$]] for Zn on a Li site assuming the known structure of LiNbO$_3$ and a typical overall broadening ($\sigma^2 = 0.0036$ Å^2). The FFT window was 3.5–13.7 Å^{-1}, Gaussian broadened by 0.3 Å^{-1}. Here and in other r-space plots, the fast oscillation is the real part R of the FFT while the envelope is $\pm\sqrt{R^2 + I^2}$ where I is the imaginary part of the FFT. The vertical solid (green) line near 2.8 Å shows the location of the strong first Zn-Nb peak (actual distance about 3.1 Å).
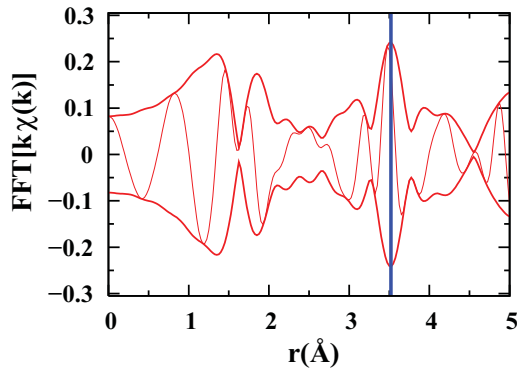
FIG. 5. (Color online) A simulation of the Zn EXAFS r-space data for Zn on a Nb site assuming the known structure of LiNbO$_3$ and a typical overall broadening ($\sigma^2 = 0.0036$ Å^2). The vertical solid (blue) line shows the location of the first Zn-Nb peak (actual distance above 3.77 Å). Note that the amplitude is low from 2.5 to 3 Å where the strongest Zn-Li peak occurs. This is a result of the very low backscattering from Li, which has only three electrons (or two for a +1 ion).

a slit height of 0.3 mm gives an energy resolution of $\delta E \sim 2.0$ eV.

Zn-doped LiNbO$_3$ crystals were purchased from Impex High Tech, Germany, with nominal (melt) Zn concentrations from 5 to 9 mol %. For each concentration we received both a polished crystal and some additional material that could be powdered for the EXAFS experiments. The latter material was ground into a fine powder and passed through a 25-μm sieve. The powder was spread with a brush on Scotch tape, which preferentially holds the smallest particles; the sizes of the particles on the tape are $\leqslant 5$ μm. Two layers of tape were then pressed together to encapsulate the powder and cut into strips; these strips were then stacked together to make EXAFS samples with an appropriate absorption for each edge. The actual Zn concentration will depend on where the EXAFS samples were located within the crystal boules; typically the concentration is low at one end and high at the other. To measure the Zn concentrations, we used the ratio of the step heights in transmission at the Zn and Nb edges at the same location on the EXAFS sample; the In concentration for one sample was also measured in a similar manner. These are tabulated in Table II. No measurement of the Mg concentration could be be made because of the low x-ray energy of the Mg K edge.

The data were reduced and the k-space data $k\chi(k)$ extracted using standard techniques [RSXAP (Ref. 35)]; for the fluorescence data, a self-absorption correction was also applied.[36] Examples of the k-space data for the LiNbO$_3$:Zn sample

TABLE II. The nominal and measured concentrations from the XAS step heights in transmission for the Zn and In dopants.

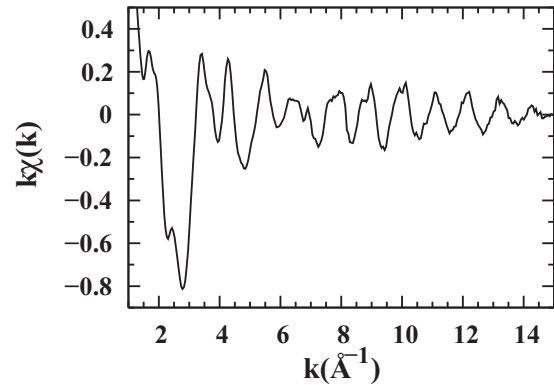| Dopant	Nominal mol %	Measured mol % (XAS)
Zn	5	7.3
Zn	7	9.6
Zn	9	11.1
In	1	0.6

FIG. 6. An example of the k-space data $k\chi(k)$ for the 11.1-mol % Zn sample at 6 K. This is an average of two scans. The signal-to-noise ratio is good out to ~ 15 Å^{-1}.

with 11.1 mol % Zn are shown in Fig. 6 to show the high signal-to-noise ratio out to $k = 15$ Å^{-1}. Next, these data were Fast Fourier Transformed into r space. Fits were carried out to the real R and imaginary I parts of the Fast Fourier Transform (FFT) using the EXAFS equation for $k\chi(k)$, given by

$$k\chi(k) = \sum_i k\chi_i(k)$$
$$= \mathrm{Im} \sum_i A_i \int_0^\infty F_i(k,r) \frac{g_i(r_{0i},r)e^{i[2kr+2\delta_c(k)+\delta_i(k)]}}{r^2} dr,$$
$$A_i = N_i S_0^2.$$

Here, $g_i(r_{0i},r)$ is the pair distribution function (PDF) for atoms at a distance r_{0i} from the center atom (Zn or Nb), $F_i(k,r)$ is the backscattering amplitude, and $\delta_c(k)$ and $\delta_i(k)$ are the phase shifts from the central and ith backscattering atom potentials, respectively. The amplitude A_i is the product of the coordination number N_i from diffraction results and S_0^2, the amplitude reduction factor, which is included to correct for multielectron effects. From fits of the low-temperature data discussed below, S_0^2 is very close to 1 for the Zn edge.

IV. EXAFS DATA ANALYSIS

A. Zn K edge

Examples of the fluorescence r-space data at the Zn K edge are shown in Fig. 7 as a function of temperature for several concentrations of Zn. These figures indicate that there is little difference between samples. To show this more explicitly we plot in Fig. 8 the data for the 7.3- and 11.1-mol % samples. This plot shows that except for the first Zn-O peak, the amplitude of the remaining peaks are slightly smaller for the 11.1-mol % sample compared to the 7.3-mol % sample. This is expected as the larger dopant concentration should introduce more disorder, but the effect is quite small. Comparing the experimental data with the simulations in Figs. 4 and 5, the largest peak occurs at 2.8 Å, where the largest Zn-Nb peak occurs for Zn$_{\mathrm{Li}}$; in contrast, the amplitude is quite low near 3.5 Å, where a Zn-Nb peak would occur for Zn$_{\mathrm{Nb}}$. This indicates that the dominant substitution site for Zn is on the Li site for all concentrations. Also the positions of the Zn-O peaks are close to that for the Li site, whereas the corresponding Zn-O
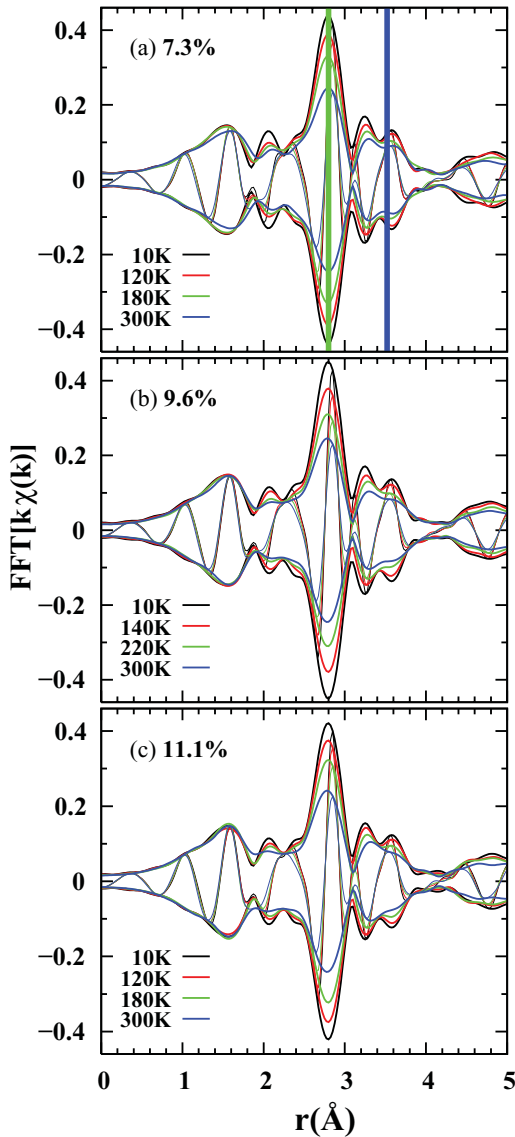
FIG. 7. (Color online) The r-space data (FFT[$k\chi(k)$]) for the 7.3-, 9.6-, and 11.1-mol % Zn samples as a function of temperature for the Zn K edge. The FFT window is 4–14.2 Å^{-1}, Gaussian broadened by 0.3 Å^{-1}. The vertical line (green) at 2.8 Å shows where the strongest Zn-Nb peak would occur for a Li substitution site while the vertical line (blue) near 3.8 Å indicates where the Zn-Nb peak would occur for a Nb site substitution. Note that the spectra for all concentrations are nearly identical indicating the same local structure, independent of concentration.

peaks for Zn$_{Nb}$ would be significantly shorter. We will start the detailed fits assuming that Li is the primary substitution site for Zn. Note that we fit each trace separately and obtain values of σ for each trace. The plotted σ^2 values are the average and the relative errors are given by the rms fluctuation; these error bars are plotted on the σ^2 vs T plots (Figs. 10 and 11). These error bars are sometimes smaller than the point symbols and are usually consistent with fluctuations from one temperature to another. Significant systematic errors also exist, which should be approximately the same for all temperatures.

It is important to recognize that when fitting r-space data, we fit to the real R and imaginary I (not shown) parts of the
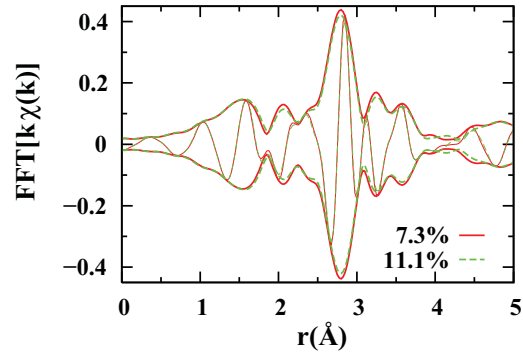

FIG. 8. (Color online) A comparison of the Zn K-edge r-space data at 10 K for the 7.3- and 11.1-mol % samples. The amplitudes of most of the peaks are slightly smaller for the 11.1-mol % sample indicating slightly more static disorder. Same FFT range as for Fig. 7.

FFT. Because of the oscillatory behavior there is interference between neighboring peaks. For example, the dip near 1.8 Å is the result of destructive interference between the first two Zn-O peaks; similarly, the sharp dip near 3.1 Å arises from interference between the first two Zn-Nb shells. The plots in Fig. 7 also show that the T dependence of the shortest Zn-O peak is very weak indicating a very stiff spring constant. The strong temperature dependence of the Zn-Nb peaks (2.5–3.6 Å) is also clear. What is less clear is that the second Zn-O peak also has a strong temperature dependence that is partially masked by the interference dip.

The detailed fits were carried out in r space to a sum of theoretical EXAFS functions, calculated for each atom pair using the program FEFF8.[34] The FFT range was 4–14.2 Å^{-1} and the fit range in r was 1.2–4.2 Å; using Stern's criteria,[37] there are then 23 independent data points. The two Zn-Nb peaks at 3.06 and 3.07 Å for the first Nb shell were treated as one peak with an amplitude of four neighbors. Also in the first fits of the low-T data, the Zn-O distances for the two further O shells of neighbors, at 3.29 and 3.43 Å, always collapsed together. Consequently, for the remainder of the fits these shells were treated as one peak with six neighbors. In addition, several multiscattering (MS) paths must be considered. Most were small but two multiscattering functions were also included. For each peak the number of neighbors was fixed to the values for the Li site and the parameters Δr and the pair distribution width σ varied. The final fits included three Zn-O shells, three Zn-Nb shells, a Zn-Li shell, plus the MS peaks; however, there are not enough degrees of freedom to allow all these parameters to vary independently, based on Stern's criteria above.[37] Consequently, some constraints must be included.

In addition, one additional parameter, ΔE_0, must be included; it describes the difference in edge energy between the value defined for the data (energy at half edge height) and the theoretical functions (for which $k = 0$ at E_0). This parameter is best defined at low T where the data are largest at high k. We fit the first three peaks for six to nine scans at low T, with ΔE_0 allowed to vary, and then obtained an average value for ΔE_0; this value was then held fixed for the fits at higher temperatures. We also set $S_o^2 = 1$ based on fits to the first three peaks at low T.
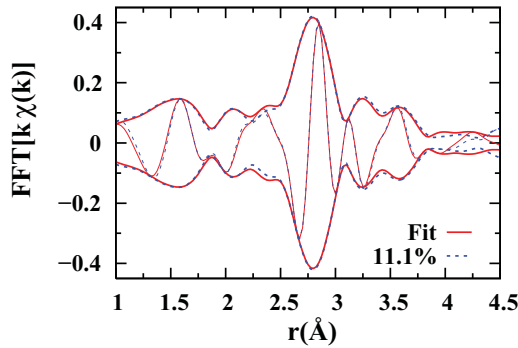
FIG. 9. (Color online) An example of a fit for the 11.1-mol % sample; the FFT window is 4–14.2 Å^{-1}, Gaussian broadened by 0.3 Å^{-1}, and the fit range in r was 1.2–4.2 Å.
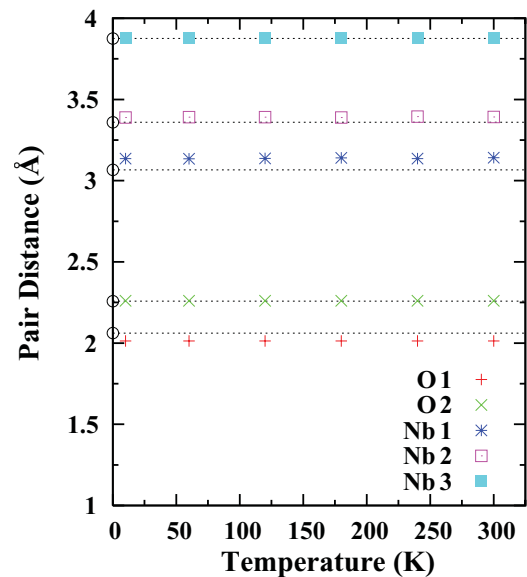

FIG. 10. (Color online) Plot of the pair distances for the first two O neighbors and the first three Nb shells about Zn as a function of T for 11.1 mol % Zn; the pair distances at low T for the Li site in LiNbO$_3$ are shown as dotted lines. The largest changes are for the first Zn-O and Zn-Nb peaks; at high r, the distances are very close to the values about a Li site in congruent LiNbO$_3$.

Constraints are particularly important for larger values of r, for which there are more overlapping peaks. In a series of test fits, we found that the more distant neighbors had distances that were very consistent with the local structure of LiNbO$_3$; consequently we constrained several of the longer pair distances to be consistent with the structure. We also constrained σ and Δr for the MS peaks to corresponding single-scattering peaks. This left 17 parameters to be varied, well below the number of independent parameters—23.

An example of a fit assuming substitution on the Li site is shown in Fig. 9 for the 11.1-mol % sample at 10 K. Fits for other concentrations are similar. The data are well described by Zn$_{Li}$, with a slight distortion of the positions of the first few shells. The main result is that the Zn-O shells are slightly contracted while the Zn-Nb shells are expanded, with the largest changes in r occurring for the first Zn-O peak and first Zn-Nb peak. This is expected from Coulomb attraction/repulsion when a +2 valent ion replaces a +1 valent ion. Further details of the low-T fits are given in Table III, and plots of the pair distances as a function of T are shown in Fig. 10 for the first two O neighbors and the three Nb shells. We also show the pair distances for congruent LiNbO$_3$ (open circles on the Y axis and as horizontal dotted lines), for comparison. Note that there is very little T dependence and that the second Zn-O peak does not shift significantly. This O neighbor is strongly bonded to two Nb^{+5} neighbors, which move away from Zn^{+2}. Thus the lack of a significant change for the second oxygen atom is a combination of attraction

toward Zn^{+2} and the outward displacement of the Nb atom pulling this O away from Zn.

There are no reported distances calculated around a Zn$_{Li}$ site in LiNbO$_3$; however, based on the work of Araujo *et al.*[8] for Zn on a Li site compensated by a Li vacancy, a similar behavior is observed; the Nb atoms are repelled while the O atoms are attracted to the Zn atom.[38] The first two calculated Zn-Nb distances are in good agreement with the EXAFS results in Table III, while the first Zn-O shell is contracted more evenly; both calculated Zn-O distances have comparable contractions that are smaller than the measured contraction for Zn-O1 (Zn-O2 shows no contraction in the EXAFS analysis). Considering the simplicity of the model with no dynamics included, this is surprisingly good agreement.

In Fig. 11 we plot σ^2 extracted from these fits (points) as a function of temperature for the first three shells of neighbors—two Zn-O shells and the first Zn-Nb peak. The Zn-O1 peak has the weakest T dependence consistent with Fig. 7, while that for

TABLE III. Fit results for 10-K data for the 7.3-, 9.6-, and 11.1-mol % samples. The Zn-O3 shell represents two Zn-O shells (three neighbors each at 3.29 and 3.43 Å; r average, 3.36 Å), which collapse to a single peak with six O neighbors at the average distance. The second column gives corresponding pair distances about the Li site for congruent LiNbO$_3$. The errors for r are ± 0.01 Å and most relative errors for σ^2 are ± 0.0005 Å^2. However, there are correlations between the σ^2's for Zn-O1 and Zn-O2 and the σ^2 errors for Zn-O2 are about 0.001 Å^2.

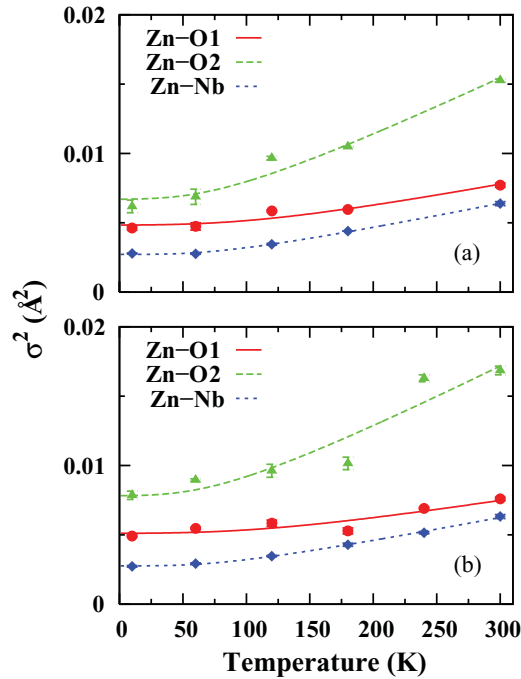| LiNbO$_3$		7.3 mol %		9.6 mol %		11.1 mol %	
Atom pair	r	r (Å)	σ^2 (Å^2)	r (Å)	σ^2 (Å^2)	r (Å)	σ^2 (Å^2)
Zn-O1	2.06	2.01	0.0046	2.01	0.0051	2.01	0.0050
Zn-O2	2.26	2.26	0.0062	2.26	0.0083	2.26	0.0082
Zn-Nb1	3.06	3.13	0.0028	3.13	0.0027	3.13	0.0028
Zn-O3	3.29	3.29	0.0043	3.29	0.0058	3.30	0.0060
Zn-Nb2	3.36	3.39	0.0044	3.40	0.0034	3.39	0.0058

FIG. 11. (Color online) Plots of σ^2 (points) as a function of T for the first three shells—two Zn-O shells and the Zn-Nb shell; (a) 7.3 mol %, (b) 11.1 mol %. The results are nearly the same for the first Zn-O and the Zn-Nb peaks, only a small increase in static disorder as the Zn concentration increases. The second Zn-O peak has a much stronger T dependence indicating a much weaker spring constant; this peak has a larger increase in the static disorder with increasing Zn concentration. These data were fit to a correlated Debye model, shown by solid or dotted lines.

the Zn-O2 peak is the largest. We fit these data to a correlated Debye model where σ^2 is given by

$$\sigma_{cD}^2 = \frac{3\hbar}{2M_R} \int_0^{\omega_{cD}} \frac{\omega}{\omega_{cD}^3} C_{ij} \coth\left(\frac{\hbar\omega}{2k_B T}\right) d\omega,$$

where ω_{cD} is the correlated Debye frequency, C_{ij} is a correlation function given by $1 - \sin(\omega r_{ij}/c)/(\omega r_{ij}/c)$, $c = \frac{\omega_{cD}}{k_D}$ where k_D is the Debye wavenumber, and M_R is the reduced mass of the atom pair. Note that ω_{cD} is not the same as the Debye temperature from other measurements such as specific heat; it is higher and a measure of the effective spring constant. It is particularly useful in comparing various bond strengths within the same sample.

The lines in Fig. 11 are fits to the correlated Debye model. The correlated Debye temperature (obtained from ω_{cD}) and static offset σ_{static}^2 are tabulated for each pair in Table IV. The values of Θ_{cD} for the two samples are the same for each atom pair within the estimated errors. Note the high value of Θ_{cD} for Zn-O1 ($\sim$600 K), which indicates a very strong bond. The static offsets are very small for the Zn-Nb peak and fairly small for the Zn-O peaks; σ_{static}^2 for the latter does increase with the Zn concentration as expected.

We next considered other possibilities such as clustering of Zn defects and a small fraction of Zn on a Nb site. For the clustering we only considered the 11.1-mol % sample and included a small Zn-Zn peak at the Zn-Li distance, 3.77 Å. For this concentration there should be $\sim$0.7 Zn atoms at

TABLE IV. Correlated Debye temperature and static offset (σ_{static}^2) for the Zn-O1, Zn-O2, and Zn-Nb pairs, for the 7.3- and 11.1-mol % samples. Relative errors from fits indicated by numbers in parentheses. Because of the high Θ_{cD} for Zn-O1, the results for this peak are very sensitive to small errors in the 300-K data, and systematic errors are likely larger.

Atom pair	7.3 mol %		11.1 mol %	
	Θ_{cD} (K)	σ_{static}^2 (Å^2)	Θ_{cD} (K)	σ_{static}^2 (Å^2)
Zn-O1	565(40)	0.0015(5)	613(71)	0.0021(7)
Zn-O2	378(20)	0.0013(8)	368(36)	0.0023(17)
Zn-Nb1	359(5)	0.0004(1)	366(5)	0.0005(1)

this distance. Such a peak is small and did not significantly change the overall fit—in fact the fit was very slightly worse, although there are more parameters. If the number of neighbors was allowed to vary, it was reduced towards zero. When we attempted to include significantly more Zn neighbors (1–3), the fit quality decreased further. Thus the number of Zn neighbors is <1 and any clustering of Zn atoms is small.

For a small partial substitution of Zn on the Nb site the amplitude of the Zn-Nb peak near 2.8 Å would decrease and a new small Zn-Nb peak (for Zn on a Nb site) would be present near 3.77 Å. Also, the Zn-O peaks for a Nb site are at shorter lengths and this would broaden the experimental Zn-O peaks. A full fit for the two different substitution sites is not possible as it would require far too many parameters. However, we could check on the effect of reducing the Zn-Nb peak at 2.8 Å and adding a corresponding small Zn-Nb peak near 3.77 Å. Such fits show that the fraction of Zn on Nb was <5%.

B. Nb K edge

The reduction and analysis for the Nb K-edge data are similar to that described above for the Zn K-edge results, but we expect a closer agreement between the EXAFS pair distances and the results from diffraction for congruent LiNbO$_3$.[13,39–41] In Fig. 12 we plot the Nb K-edge r-space data at 10 K for the 7.3- and 11.1 mol % Zn samples and compare with similar data for a 2.5-mol % Mg sample (another +2 dopant) and a 0.6-mol % In sample (+3 dopant). The data for the four samples agree very well—there is slightly more amplitude at the 3.3-Å peak for the Mg-doped sample indicating that slightly less static distortion is present. The nearly identical structure for both very dilute dopants and the 11.1-mol % Zn-doped sample indicates that the local structure about most of the Nb does not change significantly for these dopant levels.

A comparison of the data with Fig. 5 (EXAFS calculated for the Nb site) shows the expected structure about a Nb site—a double oxygen peak between 1 and 2 Å, and the peak for the Nb neighbors between 3 and 4 Å; note that the EXAFS for a Nb central atom is quite different from that for the Zn_{Li} site. In particular, a comparison of Fig. 12 with Fig. 7 shows that the first Nb neighbor peak in the Nb K-edge data (near 3.35 Å on the EXAFS plot) is considerably further away from the central Nb atom than a Nb neighbor is from Zn on a Li site (at 2.8 Å).
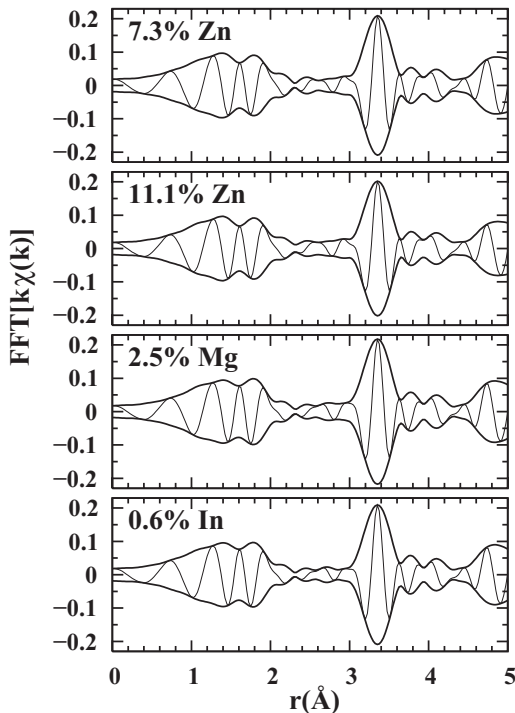
FIG. 12. Comparison of the Nb K-edge data for LiNbO$_3$ samples doped with 7.3 and 11.1 mol % Zn, together with the corresponding Nb data for another divalent dopant Mg^{+2} and In^{+3}. The four traces are nearly identical, with the data for the Mg-doped sample slightly higher near 3.3 Å. The FFT range is 4.5–15 Å^{-1}, Gaussian broadened by 0.3 Å^{-1}.
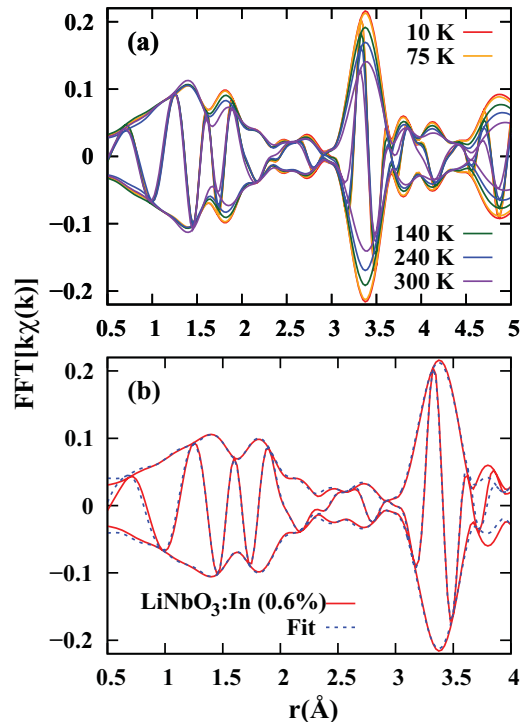

FIG. 13. (Color online) (a) The temperature dependence of the Nb K-edge r-space data for the 0.6-mol % In-doped sample. Note that there is little change of the first Nb-O peak near 1.5 Å, while the second Nb-O and Nb-Nb peaks show significant changes. The weak structure between 2.3 and 3 Å is a sum of weak Nb-Li and Nb-O peaks plus multiscattering peaks. (b) An example of a fit of the 10-K data for this sample from 1.2 to 3.7 Å; note the shorter r range for plotting this fit. Same FFT range as in Fig. 12.

In Fig. 13(a) we plot the r-space data at the Nb K edge as a function of temperature for the lowest doped sample, 0.6 mol % In. This should be closest to the pure congruent material. The amplitude for the first Nb-O peak is nearly constant, but that for the second Nb-O peak and the large Nb-Nb peak [near 3.35 Å in Fig. 13(a)] decrease significantly by 300 K.

We carried out a detailed fit of the Nb K-edge data for the 0.6-mol % In sample over the r range 1.2–3.7 Å as a function of temperature, and for the other samples only for 10 K. Here we used two Nb-O peaks ($r \sim 1.87$ and 2.14 Å), the strong Nb-Nb peak (~ 3.77 Å), plus several smaller peaks: two weak Nb-Li peaks (~ 3.06 and 3.36 Å), some longer Nb-O peaks (3.62, 3.73, and 3.87 Å), and several multiscattering peaks. For all peaks, the amplitudes (coordination numbers) were constrained to the known structure. In addition the pair distances for the weak peaks were constrained to the Nb-Nb peak distance and the LNO structure such that only an overall lattice parameter change could occur. In the first fits only 12 parameters were varied (mostly σ's)—well below the number of independent data points (20) calculated based on Stern's criteria.[37] We obtained a good fit except for $r \sim 1.9$–2.2 Å; here there is a small but significant deviation and the difference between the fit and the data appeared similar to a Nb-O peak, with $r \sim 2.5$ Å. We therefore added an additional Nb-O with a low amplitude (<1 neighbor) to the fit with σ constrained equal to that of the second Nb-O peak (σ_2) and obtained an excellent fit with 14 parameters. An example of this fit at 10 K

is shown in Fig. 13(b); in Table V we compare the results for the 0.6-mol % In and 11.1-mol % Zn samples. The two short O peak distances and the strong Nb-Nb peak distance agree to better than 0.01 Å with diffraction results. Similar fits of the Nb K-edge were obtained for the other Zn- and Mg-doped samples. The distances agree well with diffraction over the entire temperature range—there is little thermal expansion; see Fig. 14. For the 11.1%-Zn sample we added a small Nb-

TABLE V. Results for the main peaks in fits of the 10-K Nb K-edge data for 0.6-mol % In and 11.1-mol % Zn. We also include the first small Nb-Li peak and the interstitial Nb-O peak (~ 0.65–0.9 neighbors). The first column gives the results from diffraction. For this fit, the amplitudes of the main peaks are fixed to the ratio of the coordination numbers and $S_o^2 = 0.9$. The errors on the positions for the main peaks are ± 0.01 Å, while the relative errors in $\sigma^2 \sim 0.0003$ Å^2, except for the Nb-Li peaks.

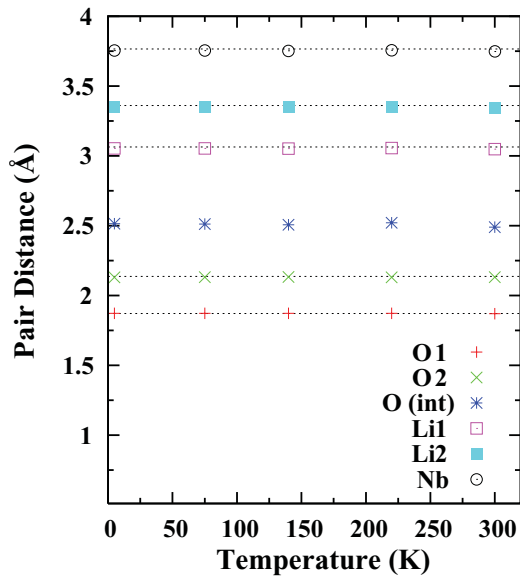| LiNbO$_3$		0.6 mol % In		11.1 mol % Zn	
Atom pair	r	r (Å)	σ^2 (Å^2)	r (Å)	σ^2 (Å^2)
Nb-O1	1.87	1.87	0.00286	1.87	.002927
Nb-O2	2.14	2.13	0.00250	2.13	.002859
Nb-Li	3.06	3.05	0.00910	3.05	.005720
Nb-Nb1	3.77	3.75	0.00264	3.76	.002992
Nb-O(int)		2.51	0.00313	2.51	.004316

FIG. 14. (Color online) The pair distances around Nb from Nb K-edge data, for the 0.6-mol % In sample. Except for the possible interstitial peak, the pair distances agree well with diffraction at low T (dotted lines) to better than 0.01 Å for all pairs, except for the weak Nb-Li peaks (0.02 Å).

Zn peak (random occupation); the quality of the fit was not too sensitive to the fraction used but did modify σ^2 for the overlapping weak Nb-Li peaks. Thus, σ^2 for the weak Nb-Li peaks has a large uncertainty in Table V.

In Fig. 15 we plot an expanded view of the O shell for the Nb K-edge data for the 11.1-mol % Zn sample, from roughly 1 to 2.4 Å, showing the data (red), the fit (green), and the fit with only two Nb-O peaks (black), which has a dip near 2.05 Å. The three individual Nb-O peaks obtained in the fits (and the sum of Nb-O1 and Nb-O2) are shown in the lower panels. The plot in the middle panel shows that the oscillatory parts of the FFT are nearly out of phase for the first two Nb-O peaks (Nb-O1 and Nb-O2) and the sum is significantly smaller than the individual peaks. Further, this cancellation is large from 1.95 to 2.15 Å, which leads to the significant dip near 2.05 Å if only these two peaks are used. Just as important is the variation of the phase for R, the real part of the FFT; for the experimental data, R varies smoothly over this range with no structure, while for the sum of Nb-O1 and Nb-O2 it has a significant oscillation. The third (extra) small peak (∼0.9 neighbors when Nb-O1,2 each have three O neighbors) fills in the dip and removes this oscillation. Note that a comparable Nb-O peak (same amplitude within 10%) is present for all the higher Zn dopant levels as well as for the low concentration 0.6-mol % In and 2.5-mol % Mg samples. Thus, it appears to be a general result. Also if we keep the sum of all the O neighbors to six, the number of O3 neighbors drops to about 0.65 and the fit is only slightly worse; thus, the amplitude uncertainty is large.

It is not clear what this extra Nb-O peak means. It may correspond to an interstitial O atom present for charge compensation for both congruent LNO and divalent (or trivalent) doping on the Li site; however, the excess O is too high if one assumes three neighbors each for Nb-O1 and Nb-O2. Instead it is likely
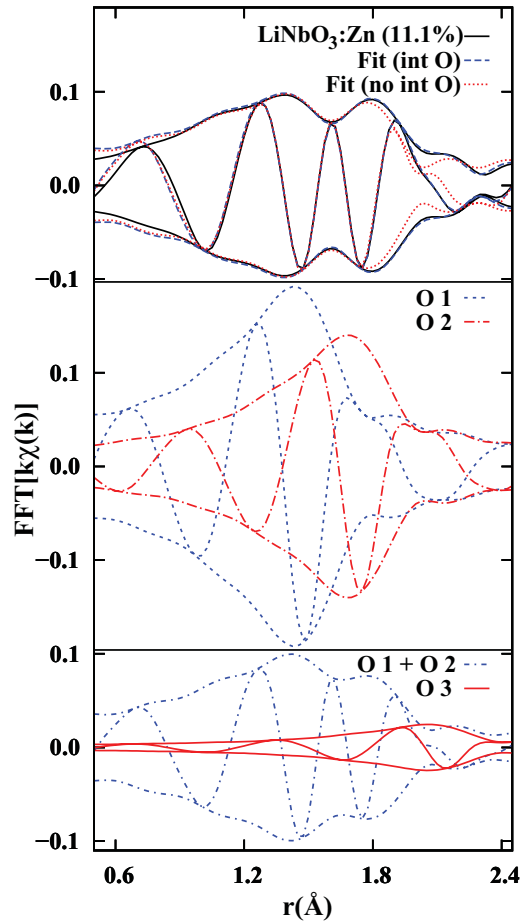

FIG. 15. (Color online) An expanded view of the Nb-O region showing the data for the 11.1-mol% Zn sample (solid black), the fit using three Nb-O peaks (dashed blue), and the fit with two peaks (dotted red)—note the dip in amplitude near 2 Å for the latter. The individual plots for Nb-O1 and Nb-O2 (with three Nb-O peaks) is plotted in the middle; the extra Nb-O3 peak plus the sum of the Nb-O1 and Nb-O2 peaks are plotted at the bottom. The first two peaks (O1 and O2) are at the expected distances for LNO; the extra peak is centered about 2.05 Å in the EXAFS plot—in the r range over which the real parts of the FFT (R) for peaks O1 and O2 are out of phase and nearly cancel as shown in second panel. Also note the phase of the real part R over this range for the data and the two fits at top.

a small distortion of the O environment about Nb, possibly related to defects found in these materials that lead to excess O, such as OH$^-$ traps[29,42,43] or O$^-$ traps,[44] or perhaps even O$_2$ defects.[45,46] The Nb-O distance will likely be longer for such defects as a result of the lower negative charge compared to O^{2-}; unfortunately, none of the studies that report OH$^-$ or O$^-$ give the concentration.

There is one caveat in interpreting this peak: we have found small but significant deviations between experiment and FEFF calculations on the high side of the first peak in many other simple systems.[47] However, the deviation here for LNO is larger and is a result of interference between the first two Nb-O peaks; even if the Nb-O standard changed slightly, the sum of two Nb-O standards split by 0.26 Å would again have a strong interference. We therefore interpret this as a small but real
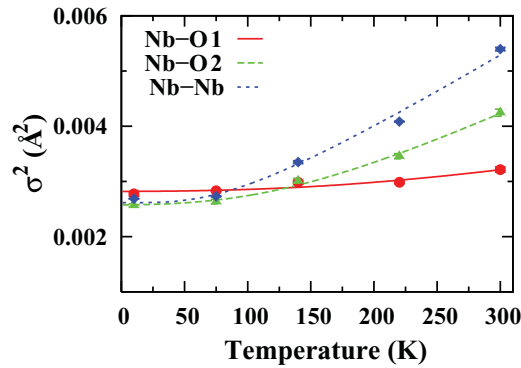
FIG. 16. (Color online) Plot of $\sigma^2(T)$ for the three largest peaks, Nb-O1, Nb-O2, Nb-Nb1 (Nb K-edge data), for the 0.6-mol % In sample. All temperature dependencies are weak indicating strong bonding, with σ^2 for the shortest Nb-O peak having the least T dependence.

structural defect involving perhaps 5–10% of the O; because of the uncertainties in the FEFF calculations and the correlations between amplitude and σ the amplitude of this peak has large errors. Further work is needed to clarify this issue.

Finally, we consider the temperature dependence of the three strongest peaks in the Nb K-edge data to ascertain the relative strength of the Nb-O1, Nb-O2, and Nb-Nb bonds. In Fig. 16 we plot $\sigma^2(T)$ for these three pairs from 10 to 300 K. In each case the T dependence is very weak (note the expanded y scale in comparison with Fig. 11), with σ^2 for Nb-O1 varying less than 0.0005 Å^2. These data were then fit to a correlated Debye model and the results tabulated in Table VI. The results confirm that the main Nb-O bonds are very strong with Nb-O1 being very rigid. Surprisingly the strongest Zn-O is only slightly weaker than the Nb-O2 bond. For LiNbO$_3$ Megaw[41] noted that the Li-O bonds are much weaker than the Nb-O bonds and viewed the structure as formed of corner sharing NbO$_6$ octahedra. Such a structure is very flexible if the Li-O bonds are weak. In LiNbO$_3$ each O has two Nb and two Li neighbors and the LiO$_6$ connect the NbO$_6$ octahedra (Li and Nb share the same O) as shown in Fig. 17; note that the Li-O bonds are nearly perpendicular to the Nb-O bonds; consequently, transverse O motion is possible if the Li-O bonds are weak. Thus when Zn replaces Li the stronger Zn-O bonds may help make the structure more rigid such that the NbO$_6$ octahedra cannot rotate or displace as easily. This may explain

TABLE VI. Correlated Debye temperatures Θ_{cD} and static distortions around the Nb site. The very large values of Θ_{cD} for Nb-O, much larger than the highest measurement temperature (300 K), means that the errors in Θ_{cD} are large ± 100 K and perhaps larger for Nb-O1. The static contribution to σ^2 for Nb-O2 is very slightly negative—but zero within our relative (repeatability) uncertainties, which are about 0.0003 Å^2.

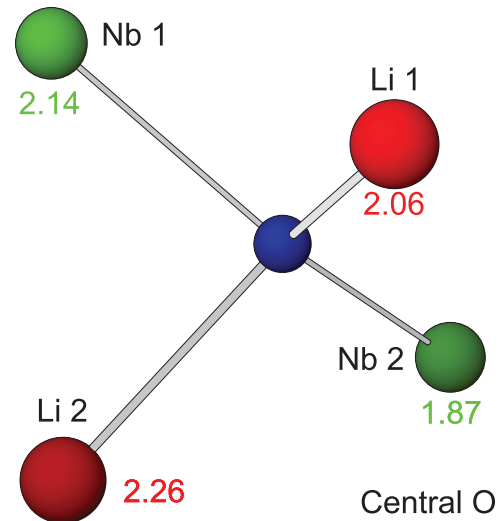| Atom pair	Θ_{cD} (K)	σ^2_{static} (Å^2)
Nb-O1	1162	0.00135
Nb-O2	725	−0.00006
Nb-Nb1	402	0.0007

FIG. 17. (Color online) The environment about the O atoms showing the Nb-O-Li angles and Nb-O and Li-O bonds. Nb1-O-Nb2, 139.9°; Li1-O-Li2, 121.3°; Li1-O-Nb1, 93.8°; Li1-O-Nb2, 117.3°; Li2-O-Nb1, 88.1°; Li2-O-Nb2, 95.4°. Note that the Li-O bonds (and Zn-O bonds around Zn) are roughly perpendicular to the Nb-O bonds.

the sudden decrease of the photorefractive index to zero when sufficient Zn's are on the Li sites.

V. DISCUSSION AND CONCLUSIONS

The Zn K-edge EXAFS measurements and analysis for LiNbO$_3$:Zn are only consistent with Zn substitution on or very near to the Li site. As the Zn concentration changes from 7.3 to 11.1 mol % the EXAFS r-space function changes very little. A slight amplitude reduction reflects an increased local disorder for increasing Zn concentration. In the fits we also considered the possibility of some fraction of the Zn on an Nb site—such Zn atoms would have a large Zn-Nb peak at 3.77 Å—where a weak Zn-Li peak occurs for Zn$_{\text{Li}}$. Because of the unusually large difference in amplitudes between Zn-Li and Zn-Nb (see Fig. 3) EXAFS is very sensitive to a small fraction of Zn$_{\text{Nb}}$; our data are consistent with no Zn on Nb sites, but an upper limit is 5% Nb site occupation.

We also considered clustering of Zn$_{\text{Li}}$ defects—in which case the number of Zn neighbors at 3.77 Å would be between 1 and 2. Again, because of the very small Zn-Li peak amplitude compared to that for a Zn-Zn peak, a small cluster of Zn would produce a significant Zn-Zn peak, which is not observed. The fits are not sensitive to small amounts of Zn but are inconsistent with more than one Zn neighbor; thus all our data are inconsistent with a significant clustering of Zn that is needed for some defects such as five Zn$_{\text{Li}}$ surrounding a Nb vacancy.[23]

The detailed analysis also shows that the three nearest O neighbors to Zn (first peak) are slightly pulled inward by 0.05 Å while the nearest Nb metal atoms are pushed away by 0.07 Å; further O and Nb shells have a similar but smaller displacement. Calculations for Zn on a Li site plus a Li vacancy show similar behavior.[38] Overall, the environment about Zn is expanded out to ~± 4 Å. Because we probe bond lengths relative to the Zn atom it is difficult to determine

if or how much the Zn atom might be displaced from the ideal Li site. However, referring to Fig. 1, both the Nb above and below the Zn$_{Li}$ are pushed away, but by different amounts—difference about 0.04 Å. Thus any displacement of Zn$_{Li}$ from the crystallographic site should be small. However, even a small displacement such as 0.04 Å would modify the local polarization and, together with the other displacements and strong Zn-O bonds, will be important for modeling how the defects modify the optical properties as calculated for example, by Xue and co-workers.[7,9,10]

The expansion of the Nb atoms about the Zn$_{Li}$ defect likely contributes to the observed increase in lattice constants[17,19,21,30] for high Zn concentrations. Because Li is a very weak backscatterer and the amplitude of the rather long Zn-Li peak is very low, it is hard to establish if there are vacancies on the Li sites.

The first Zn-O peak has a weak temperature dependence and corresponds to a very stiff Zn-O bond (i.e., stiff spring) with a correlated Debye temperature Θ_{cD} of order 600 K (here Θ_{cD} is not the usual Debye temperature and is a measure of the bond strength). In contrast, the second Zn-O2 peak, has a larger temperature dependence indicating a weaker effective spring constant. Note that all O atoms are very strongly bonded to Nb, and in the Nb K-edge data the thermal vibrations are described by even larger Θ_{cD}, $\sim$1100 and 725 K. Although in LiNbO$_3$ the NbO$_6$ octahedra are relatively free to rotate because of weak Li-O bonds, when Zn is added the Zn-O bonds are quite strong and likely stiffen the lattice when sufficient Zn is present. This may explain the decrease of the photorefractive index near 7 mol % Zn.

The fact that Zn is primarily on the Li site and forms a significant local distortion needs to be considered to understand how Zn changes the optical properties of LNO. We anticipate that these more detailed local structure measurements will stimulate further theoretical investigations of the environment about Zn, particularly the pair distances, which are crucial for understanding how Zn and other dopants modify the optical properties.

[1] F. Xin, G. Zhang, F. Bo, H. Sun, Y. Kong, J. Xu, T. Volk, and N. M. Rubinina, J. Appl. Phys. **107**, 33113 (2010).

[2] T. Volk and M. Wohlecke, in *Lithium Niobate: Defects, Photorefraction and Ferroelectric Switching* (Springer, New York, 2008), pp. 2–4.

[3] X. Zhen, Q. Li, and Y. Xu, Cryst. Res. Technol. **41**, 276 (2006).

[4] U. Schlarb and K. Betzler, Phys. Rev. B **50**, 751 (1994).

[5] F. Abdi, M. Aillerie, P. Bourson, and M. D. Fontana, J. Appl. Phys. **106**, 33519 (2009).

[6] H. Donnerberg, S. M. Tomlinson, C. R. A. Catlow, and O. F. Schirmer, Phys. Rev. B **44**, 4877 (1991).

[7] D. Xue, K. Betzler, and H. Hesse, Opt. Commun. **182**, 167 (2000).

[8] R. M. Araujo, K. Lengyel, R. A. Jackson, L. Kovacs, and M. E. G. Valerio, J. Phys.: Condens. Matter **19**, 46211 (2007).

[9] X. He and D. Xue, Opt. Commun. **265**, 537 (2006).

[10] Y. He and D. Xue, J. Phys. Chem. C **111**, 13238 (2007).

[11] H. Xu, D. Lee, J. He, S. B. Sinnott, V. Gopalan, V. Dierolf, and S. R. Phillpot, Phys. Rev. B **78**, 174103 (2008).

[12] H. Xu, D. Lee, S. B. Sinnott, V. Dierolf, V. Gopalan, and S. R. Phillpot, J. Phys.: Condens. Matter **22**, 135002 (2010).

[13] D. Lee, H. Xu, V. Dierolf, V. Gopalan, and S. R. Phillpot, Phys. Rev. B **82**, 014104 (2010).

[14] H. Xu, A. Chernatynskiy, D. Lee, S. Sinnot, V. Dierolf, V. Gopalan, and S. Phillpot, Phys. Rev. B **82**, 184109 (2010).

[15] C. Zaldo, C. Prieto, H. Dexpert, and P. Fessler, J. Phys.: Condens. Matter **3**, 4235 (1991).

[16] C. Prieto and C. Zaldo, J. Phys.: Condens. Matter **6**, L677 (1994).

[17] F. Abdi, M. Aillerie, M. Fontana, P. Bourson, T. Volk, B. Maximov, S. Sulyanov, N. Rubinina, and M. Wohlecke, Appl. Phys. B **68**, 795 (1999).

[18] T. Volk, N. Rubinina, and M. Wohlechke, J. Opt. Soc. Am. B **11**, 1681 (1994).

[19] T. S. Chernaya, B. A. Maksinov, T. R. Volk, N. M. Rubinina, and V. I. Simonov, JETP Lett. **73**, 103 (2001).

[20] Y. Zhang, Y. H. Xu, M. H. Li, and Y. Q. Zhao, J. Cryst. Growth **233**, 537 (2001).

[21] T. Volk, B. Maximov, S. Sulyanov, N. Rubinina, and M. Wohlecke, Opt. Mater. **23**, 229 (2003).

[22] C.-T. Chia, C.-C. Lee, P.-J. Chang, M.-L. Hu, and L. J. Hu, Appl. Phys. Lett. **86**, 182901 (2005).

[23] P.-C. Tsai, M.-L. Sun, C.-T. Chia, H.-F. Lu, S.-H. Lin, M.-L. Hu, and J.-F. Lee, Appl. Phys. Lett. **92**, 161902 (2008).

[24] P.-C. Tsai, C.-T. Chia, S.-T. Lin, Y.-C. Huang, H.-F. Lu, and S.-H. Lin, Appl. Phys. Lett. **94**, 81909 (2009).

[25] S. Fang, Z. Han, Y. Qiao, Y. Liu, and Q. Jia, Cryst. Res. Technol. **44**, 1211 (2009).

[26] A. V. Yatsenko, S. V. Yevdokimov, D. Y. Sugak, and I. M. Solskii, Acta Phys. Pol. A **117**, 166 (2010).

[27] T. S. Chernaya, T. R. Volk, I. A. Verin, and V. I. Simonov, Cryst. Rep. **53**, 573 (2008).

[28] L. Kovács, L. Rebouta, J. C. Soares, M. F. da Silva, M. Hage-Ali, J. P. Stoquert, P. Siffert, C. Zaido, Z. Szaller, and K. Polgár, Mater. Sci. Eng. B **9**, 505 (1991).

[29]L. Kovács, M. Wöhlecke, A. Jovanović, K. Polgár, and S. Kapphan, J. Phys. Chem. Solids **6**, 797 (1991).

[30]L. Zhao, X. Wang, B. Wang, W. Wen, and T.-Y. Zhang, Appl. Phys. B **78**, 769 (2004).

[31]K. H. Kim, K. B. Shim, and K. H. Auh, Mater. Lett. **55**, 116 (2002).

[32]S. Sulyanov, B. Maximov, T. Volk, H. Boysen, J. Schneider, N. Rubinina, and T. Hansen, Appl. Phys. A **74**, S1031 (2002).

[33]T. Volk, B. Maximov, T. Chernaya, N. Rubinina, M. Wöhlechke, and V. Simonov, Appl. Phys. B **72**, 647 (2001).

[34]A. L. Ankudinov, B. Ravel, J. J. Rehr, and S. D. Conradson, Phys. Rev. B **58**, 7565 (1998).

[35]See [http://lise.lbl.gov/RSPAK].

[36]C. H. Booth and F. Bridges, Phys. Scr. **T115**, 202 (2005).

[37]E. A. Stern, Phys. Rev. B **48**, 9825 (1993).

[38]R. A. Jackson (private communication).

[39]S. C. Abrahams, J. M. Reddy, and J. L. Bernstein, J. Phys. Chem. Solids **27**, 997 (1966).

[40]S. C. Abrahams, H. J. Levinstein, and J. M. Reddy, J. Phys. Chem. Solids **27**, 1019 (1966).

[41]H. D. Megaw, Acta Crystallogr. Sect. A **24**, 583 (1968).

[42]F.-Y. Guo, Q. Lu, L. Sun, H.-T. Li, X.-H. Zhen, Y.-H. Xu, and L.-C. Zhao, Mater. Sci. Eng. B **131**, 267 (2006).

[43]P.-C. Tsai, H.-F. Lu, P.-J. Chang, C.-T. Chia, H.-L. Liu, S.-H. Lin, and M.-L. Hu, Jpn. J. Appl. Phys. **46**, 7159 (2007).

[44]H. Qiao and Y. Tomita, Opt. Express **14**, 5773 (2006).

[45]S. Limpijumnong, X. Li, S.-H. Wei, and S. B. Zhang, Appl. Phys. Lett. **86**, 211910 (2005).

[46]P. Erhart, K. Albe, and A. Klein, Phys. Rev. B **73**, 205203 (2006).

[47]Z. Kvitky, F. Bridges, and G. van Dorssen, Phys. Rev. B **64**, 214108 (2001).